

## Compound pendulum model of a moored heaving buoy

Jana Orszaghova<sup>1</sup>, Hugh Wolgamot<sup>1</sup>, Jørgen Hals Todalshaug<sup>2</sup>, Hervé Gaviglio<sup>2</sup>

<sup>1</sup> Oceans Graduate School and Wave Energy Research Centre, University of Western Australia, Australia.

<sup>2</sup> CorPower Ocean, Stockholm, Sweden.

jana.orszaghova@uwa.edu.au, hugh.wolgamot@uwa.edu.au, jorgen.hals@corpowersocean.com,

herve.gaviglio@corpowersocean.com

### INTRODUCTION

Parametric resonance is a phenomenon that can arise in mechanical systems, whereby a response in a particular mode is excited via a time-varying parameter, as opposed to via direct forcing. A well-known example in ocean engineering is the parametric roll of ships. Such dynamic instability can arise due to non-linear coupling between different motion modes. For this reason, wave-activated wave energy converters (WECs), which are free to move in multiple degrees of freedom (DoF), are particularly prone to such dynamic instabilities.

We consider an axi-symmetric multi-body system, which consists of two rigid components (the buoy and the slide), and is taut-moored (see Fig. 1). The buoy and the slide are connected via a pre-tension system as well as a negative spring mechanism which allows the system to be tuned to the incident waves and act as an effective WEC. The buoy can move along the slide, and energy is extracted from this relative motion. The rotational symmetry axes of the buoy and the slide are always aligned. Apart from this constraint, the rigid bodies can move in 6 DoF, though their dynamics are constrained by their mechanical couplings and the mooring system.

If the system is sufficiently tensioned, under the action of waves all components pivot together about the anchoring point. Thus, a simplified pendulum representation is utilised below in order to reduce the number of DoF, such that the terms in the governing equations remain tractable and a deeper understanding of the system dynamics can be gained. The proposed model is based on linear potential flow theory, but allows for non-linear hydrostatics.

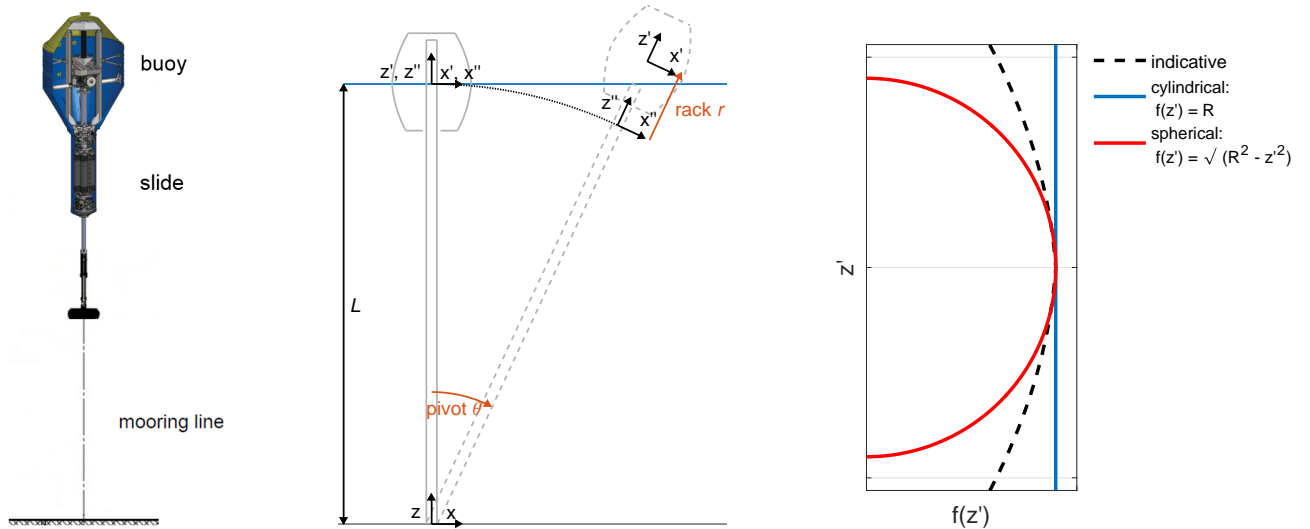


Fig. 1: Left: Full system. Middle: Simplified 2 DoF system. Right: Hull approximations.

### DERIVATION OF GOVERNING EQUATIONS

We represent the whole system via two rigid bodies: body 1 is the surface-piercing buoy, and body 2 is the submerged slide (assumed to extend to the sea bed), see Fig 1. Only 2 DoF are considered: the two-body system can pivot about the anchor point, and this motion mode is denoted by  $\theta$ . Body 1 can additionally move in the instantaneous radial direction (i.e. slide along the rotational symmetry axis of

bodies 1 and 2), and this motion mode is denoted by  $r$  and referred to as the rack motion. The WEC system is thus represented as a compound pendulum with a mass-spring-damper.

As shown in Fig. 1, we define a fixed coordinate system  $(x, z)$  which is centred at the anchoring pivot point on the sea bed. The incident waves are assumed to propagate along the  $x$ -axis. We also define two moving body-fixed coordinate systems. The body 1 coordinate system  $(x', z')$  rotates and translates with the instantaneous buoy motions, and has its origin in the middle of the buoy's equilibrium waterplane area. The body 2 coordinate system  $(x'', z'')$  is fixed to the slide, and as such it follows the instantaneous rotation of body 2. The transformations between the coordinate systems are

$$\mathbf{x} = \mathbf{T}(\mathbf{x}') : \begin{pmatrix} x \\ z \end{pmatrix} = \begin{pmatrix} (L+r)\sin\theta \\ (L+r)\cos\theta \end{pmatrix} + \begin{pmatrix} \cos\theta & \sin\theta \\ -\sin\theta & \cos\theta \end{pmatrix} \begin{pmatrix} x' \\ z' \end{pmatrix}, \quad \mathbf{x} = \mathbf{T}(\mathbf{x}'') : \begin{pmatrix} x \\ z \end{pmatrix} = \begin{pmatrix} L\sin\theta \\ L\cos\theta \end{pmatrix} + \begin{pmatrix} \cos\theta & \sin\theta \\ -\sin\theta & \cos\theta \end{pmatrix} \begin{pmatrix} x'' \\ z'' \end{pmatrix},$$

where  $L$  is the vertical distance between the anchor/pivot point and the still free surface, which here is equivalent to the water depth  $h$ .

We consider conservation of angular momentum for bodies 1 and 2, and conservation of linear momentum in the instantaneous radial direction  $\mathbf{u}_r = (\sin\theta, \cos\theta)^\top$  for body 1, which give

$$m_B \frac{d^2}{dt^2} (\mathbf{T}(\mathbf{x}'_{CoG,B})) \cdot \mathbf{u}_r = m_B (\ddot{r} - (L+r+z'_{CoG,B})\dot{\theta}^2) = \mathbf{F} \cdot \mathbf{u}_r, \quad (1)$$

$$\frac{d}{dt} (I\dot{\theta}) = \ddot{\theta}I_0 + r\ddot{\theta} 2m_B(L+z'_{CoG,B}) + \dot{r}\dot{\theta} 2m_B(L+z'_{CoG,B}) + r\dot{r}\dot{\theta} 2m_B + r^2\ddot{\theta} m_B = \tau, \quad (2)$$

where  $\cdot$  denotes the dot product and  $I_0 = \sum_{i=B,S} I_{CoG,i} + (L+z'_{CoG,i})^2 m_i$  with the subscripts  $B$  and  $S$  referring to the buoy and the slide respectively. As such, for the corresponding rigid body,  $m_i$ ,  $\mathbf{x}'_{CoG,i} = (0, z'_{CoG,i})^\top$  and  $I_{CoG,i}$  denote the mass, the position vector of the centre of gravity, and the moment of inertia about an axis perpendicular to the symmetry axis and passing through  $\mathbf{x}'_{CoG,i}$ . The inertia terms have been expanded out, whereby the second expanded term in Eq. 1 represents the centrifugal force, and the 4 non-linear coupling terms in Eq. 2 arise due to the fact that the buoy can translate along the  $\mathbf{u}_r$  direction.  $\mathbf{F}$  and  $\tau$  are the external gravitational, buoyancy, power take-off and hydrodynamic forces and moments, which are discussed below.

The gravitational force and the corresponding pivoting moment are straightforward to formulate, and as such the details are omitted. The radial buoyancy force component acting on body 1 is given by

$$F_B = \rho g V(t) \cos\theta = \rho g V_B \cos\theta + \rho g \Delta V \cos\theta, \quad (3)$$

$$\text{cylindrical: } = \rho g V_B \cos\theta + \rho g S_B (L(1 - \cos\theta) - r \cos\theta),$$

$$\text{spherical: } = \rho g V_B \cos\theta + \rho g S_B \cos\theta (L(1 - \cos\theta) - r \cos\theta) - \rho g \cos\theta \frac{\pi}{3} (L(1 - \cos\theta) - r \cos\theta)^3,$$

where the instantaneous submerged volume of the buoy  $V(t)$  is decomposed into the equilibrium/static submerged volume  $V_B$  and the instantaneous additional submerged volume  $\Delta V$ . This additional volume is bounded by the body-fixed plane given by  $z' = 0$  and the still free surface given by  $z = L$ . It could be evaluated numerically from the buoy hull geometry for arbitrary  $r$  and  $\theta$ . However, here we consider an analytical approach for simplified buoy hull shapes (see Fig. 1) to understand the role of the resultant terms in the governing equations (see Eq. 3). The buoyancy pivoting moment acting on the surface-piercing body 1 can also be expressed explicitly using standard results for a cylindrical segment and a spherical cap, though the equations are more complicated. The buoyancy pivoting moment acting on the submerged body 2 is straightforward to formulate, as the buoyancy force and the centre of buoyancy (in body coordinates) do not change.

The power-take off (PTO) forces act along the  $\mathbf{u}_r$  direction, so induce no pivoting moment. The PTO forces can be parametrised as  $F_{PTO} = -(\rho g V_B - m_B g) - K_1 r - K_3 r^3 - B \dot{r}$ , where the mean component balances the buoy net/excess buoyancy,  $K_1$  and  $K_3$  represent the linear and cubic PTO stiffness coefficients and  $B$  represents linear PTO damping, which are tunable. We note that  $K_1$  is negative, which helps reduce the heave natural frequency by partly offsetting the hydrostatic stiffness

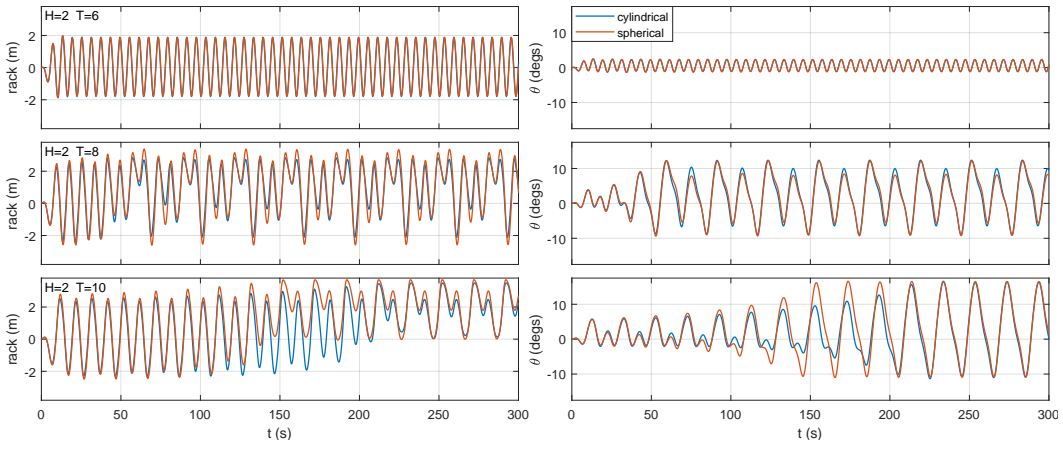


**Fig. 2: Rack  $r$  and pivot  $\theta$  motion timeseries in regular wave conditions of  $H = 2$  m and  $T = 6, 8, 10$  s.**

$\rho g S_B$  (where  $S_B = \pi R^2$  is the equilibrium waterplane area of the buoy with radius  $R$ ). We also note that the cubic term is characteristic of negative spring mechanisms. Wave induced hydrodynamic forces and moments are calculated from linear potential flow theory, with the linear hydrodynamic coefficients evaluated for the actual buoy hull geometry. We also account for viscous drag force and moment using a quadratic relative velocity formulation.

## RESULTS

The resulting system of equations is non-linear. The non-linear terms can be expanded as a Taylor series in  $r$  and  $\theta$ , which allows for an insightful analysis of the individual terms that arise at different orders. Moreover, the approximate equations also underpin development of an instability prediction model based on the Mathieu equation. The approximate third-order  $r$  equation becomes

$$\begin{aligned}
 (m_B + a_r(\infty))\ddot{r} + \int_{-\infty}^t K_{rad,r}(t-\tau)\dot{r}(\tau)d\tau + B\dot{r} + (K_1 + \rho g S_B)r \\
 - \theta^2 \frac{1}{2} (gm_B - \rho g V_B + \rho g L S_B) - \dot{\theta}^2 m_B (L + z'_{CoG,B}) - F_{drag} \\
 \text{cylindrical: } -r\dot{\theta}^2 m_B - r\theta^2 \frac{1}{2} \rho g S_B + K_3 r^3 = F_{exc,r} \quad \text{spherical: } -r\dot{\theta}^2 m_B - r\theta^2 \rho g S_B + (K_3 - \frac{\pi}{3} \rho g) r^3 = F_{exc,r}
 \end{aligned} \tag{4}$$

where the linear terms appear on the first line, and include the radiation impulse response function  $K_{rad,r}$  and the added mass at infinite frequency  $a_r(\infty)$ . The quadratic terms appear on the second line, where we identify second-order excitation-like terms proportional to  $\theta^2$  and  $\dot{\theta}^2$ . These can give rise to different harmonics in the  $r$  response: a mean offset in  $r$ , as well as motions at sum and difference frequencies of the  $\theta$  oscillations. Their effect is manifested in the  $r$  time series plots in Fig. 2 (see  $T = 8, 10$  s where the  $\theta$  motions are large). The two hull approximations begin to deviate at third order. The  $r\dot{\theta}^2$  and  $r\theta^2$  terms represent time-varying stiffness terms, while the  $r^3$  term constitutes a non-linear restoring force. The third-order  $\theta$  equation is given by

$$\begin{aligned}
 (I_0 + a_\theta(\infty))\ddot{\theta} + \int_{-\infty}^t K_{rad,\theta}(t-\tau)\dot{\theta}(\tau)d\tau + K_\theta \theta \\
 - \theta r (gm_B - \rho g V_B + \rho g L S_B) + (\dot{\theta} \dot{r} + \ddot{\theta} r) 2m_B (L + z'_{CoG,B}) - M_{drag} \\
 \text{cylindrical: } -\theta r^2 \frac{1}{2} \rho g S_B + (2\dot{\theta} r \dot{r} + \ddot{\theta} r^2) m_B + \theta^3 \left( -\frac{1}{6} K_\theta + \frac{1}{2} \rho g S_B L^2 + \frac{1}{2} \rho g S_{11} \right) = M_{exc,\theta} \\
 \text{spherical: } -\theta r^2 \rho g S_B + (2\dot{\theta} r \dot{r} + \ddot{\theta} r^2) m_B + \theta^3 \left( -\frac{1}{6} K_\theta + \frac{1}{2} \rho g S_B L^2 \right) = M_{exc,\theta}
 \end{aligned} \tag{5}$$

where  $K_\theta = \rho g S_{11} + \sum_{i=B,S} \rho g V_i (L + z'_{CoB,i}) - g m_i (L + z'_{CoG,i})$ , with  $S_{11} = \frac{\pi}{4} R^4$  and  $\mathbf{x}'_{CoB,i} = (0, z'_{CoB,i})^T$  denoting the second waterplane moment and the equilibrium centres of buoyancy respectively. At second order,  $\theta r$ ,  $\dot{\theta} \dot{r}$  and  $\ddot{\theta} r$  represent time-varying stiffness, time-varying damping and time-varying inertia components. Systems with a periodically-varying stiffness coefficient are well studied and according to Floquet theory can admit exponentially growing solutions, depending on the magnitude and frequency of this parametric excitation and the amount of linear damping (see e.g. [1]). The non-linear cubic stiffness  $\theta^3$  and the quadratic damping terms keep the growing  $\theta$  oscillations bounded (see e.g. [2] and

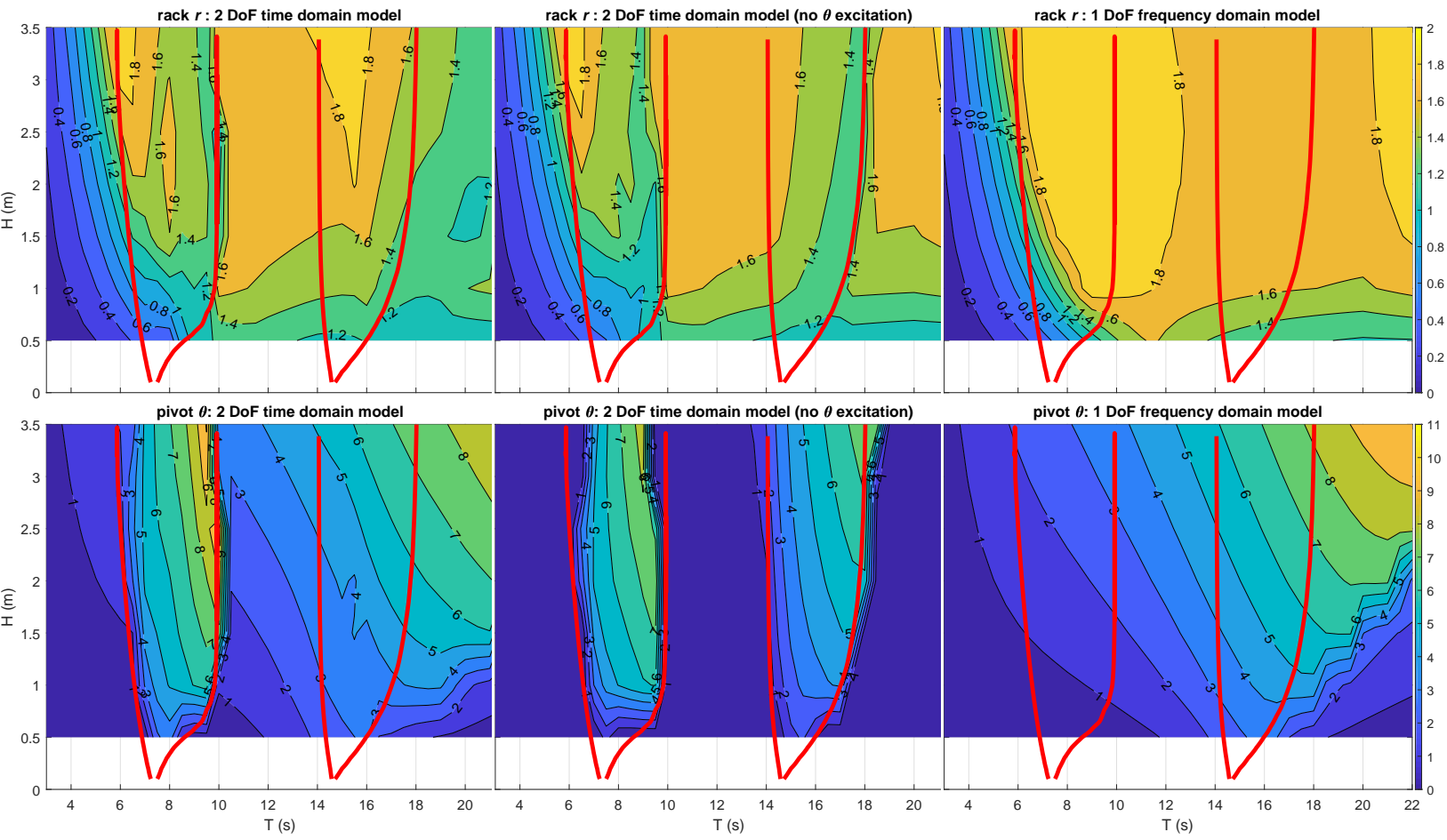


**Fig. 3: Standard deviation of rack  $r$  in m (top) and pivot  $\theta$  in degrees (bottom). Left: 2 DoF time domain model. Middle: 2 DoF model, with wave excitation in  $\theta$  suppressed. Right: 1 DoF models. Stability boundaries of the Mathieu equation are shown in red.**

[3]). We note that  $\frac{1}{2}\rho g S_{11}$  is more than two orders of magnitude smaller than the other two  $\theta^3$  coefficients combined. For this reason, the limiting amplitudes of the unstable  $\theta$  motions will not differ greatly for the two different hull approximations (see  $T = 8, 10$  s in Fig. 2).

Fig. 3 presents results from a large range of regular wave conditions. In the  $\theta$  plots, the first two instability branches are clearly seen in the time domain model results, and these can be successfully predicted by the stability boundaries of the Mathieu equation. These two branches are centered at  $T = \frac{1}{2}T_{n\theta}, T_{n\theta}$  with  $T_{n\theta} = 2\pi/\sqrt{\frac{K_\theta}{I_0+a_\theta(\omega_{n,\theta})}}$  being the pivot/pendulum natural period. The unstable  $\theta$  motions in the first branch exhibit a period-doubling response (see Fig. 2). The accompanied reduction in rack motion within the first instability branch can be seen by comparing the time domain results to the solution from a 1 DoF frequency domain  $r$  model, which approximates the rack response in the absence of coupling with  $\theta$ . The compound pendulum model gives valuable insight into the dynamics of the floating WEC, and provides an efficient tool for discovering motion instabilities in early design stages. Due to its efficiency, it can be used in studies investigating influence of different system parameters, as well as for example to find optimum PTO coefficients (as these are likely to differ under the influence of the  $\theta$  instability). At the workshop we will present further results extended to include irregular wave conditions.

JO and HW acknowledge support from the UWA Research Priorities Fund. HW acknowledges financial support from Shell Australia and from the Lloyds Register Foundation.

[1] Grimshaw, R. (1991) *Nonlinear Ordinary Differential Equations*. Taylor & Francis.  
 [2] Kovacic, I. *et al.* (2018) Mathieu's equation and its generalizations: Overview of stability charts and their features. *Applied Mechanics Reviews*, 70.  
 [3] Orszaghova, J. *et al.* (2020) Onset and limiting amplitude of yaw instability of a submerged three-tethered buoy. *Proc. of the Royal Society A*, 476.